Inorganic Chemistry
Cite This: Inorg. Chem. 2020, 59, 203−213
Article
pubs.acs.org/IC

Bridging Solution and Solid-State Chemistry of Dicyanoaurate: The Case Study of Zn−Au Nucleation Units

Emanuele Priola,*[,†] Giorgio Volpi,[†] Roberto Rabezzana,[†] Elisa Borfecchia,[†] Claudio Garino,[†] Paola Benzi,[†] Andrea Martini,[§,∥] Lorenza Operti,[†] and Eliano Diana*[,†,‡]

[†]Department of Chemistry and NIS Center, University of Turin, Via P. Giuria 7, 10125 Turin, Italy
[‡]CriSDi, Interdepartmental Center for Crystallography, Via Pietro Giuria 7, 10125 Turin, Italy
[§]Department of Physics, University of Turin, Via P. Giuria 1, 10125 Turin, Italy
[∥]International Research Institute "Smart Materials", Southern Federal University, Zorge Street 5, 344090 Rostov-on-Don, Russia

Supporting Information

ABSTRACT: The behavior in solution of the dicyanoaurate anion in the presence of other metal centers has so far been little explored, despite its importance in material science. The design and synthesis of systems with controlled coordination behavior, using chelating ligands and Zn^{II}, has allowed us to detect self-assembly and oligomerization in solution. This phenomenon has been studied with ^{13}C and ^{1}H NMR, absorption and emission UV−vis spectroscopy, ESI-MS, and XAS at both the Au L_3-edge and Zn K-edge: all of these techniques confirm the presence of Au−Zn aggregation products. These fragments, resembling structural units in the solid state, reveal that coordination of dicyanoaurate to free sites around metal centers can occur at a lower concentration than those at which crystals start to form and at which aurophilic interactions are observed, forming the connection between solution species and solid-state architectures.

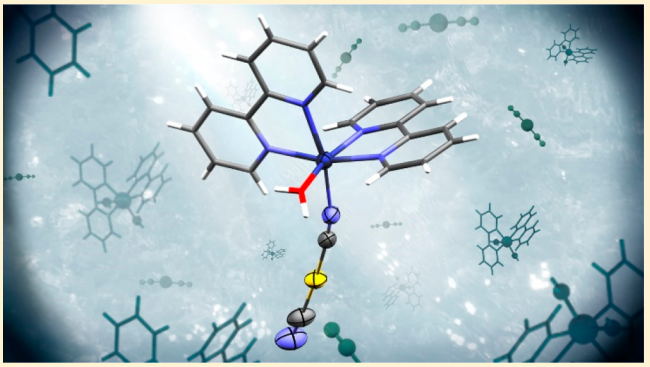

INTRODUCTION

The formation of bimetallic and trimetallic complexes by employing metalloligands is a common strategy in the preparation of crystalline supramolecular architectures.[1,2] These complexes are often the result of a "rational" use of molecular tectons, but in some cases, they seem rather to represent a serendipitous consequence of crystal packing in complex mixtures. Most reported preparations consist of a simple combination of solutions of reagents, left to stand for a long time until crystalline products are formed. Characterization is commonly carried out by SC-XRD (or NMR) in the solid state, while preorganization phenomena and assembly mechanisms of the building units in solution are very rarely addressed. Most often, reticular forces are envisaged as the main agent driving the formation of products. However, in the absence of any clue as to the reactivity in solution, it is difficult to understand in which manner a crystal engineering approach may control the passage from the solution to the crystalline state. In particular, the role played by solution-phase preorganization and the formation or the growth of nucleation units could be crucial in the rational design and realization of solid functional architectures and is currently one of the hottest research topics in supramolecular and solid-state chemistry.[3−8]

The dicyanoaurate ion is a tecton which is widely employed because of the versatility of the intermolecular interactions that it can establish: hydrogen-bond and aurophilic contacts (see, e.g., Figure 1). In addition, its linear shape favors the formation of supramolecular 1D, 2D, and 3D networks that have demonstrated interesting properties, such as phosphorescence, vapochromism, and giant negative linear compressibility (GNLC).[9−14] The complexing power of the cyanide fragment is commonly employed to synthesize heteronuclear complexes in the solid state, but the behavior of $[Au(CN)_2]^-$ in solution in the presence of other metal ions has seldom been investigated. In this contribution, we aim to demonstrate the existence of preorganization in solution, eventually driven by solvent effects and preceding the nucleation step. The work is focused on Zn−Au heteronuclear complexes, identified as model systems of nucleation units yielding to supramolecular networks. By applying a multitechnique approach, combining optical spectroscopies with NMR, ESI-MS, and XAS, we thoroughly characterized these systems, bridging their solution-phase and solid-state chemistry.

RESULTS AND DISCUSSION

Synthesis. In our endeavor to establish connections between the solution chemistry of metal complexes and a

Received: April 9, 2019
Published: December 17, 2019

DOI: 10.1021/acs.inorgchem.9b00961
Inorg. Chem. 2020, 59, 203−213

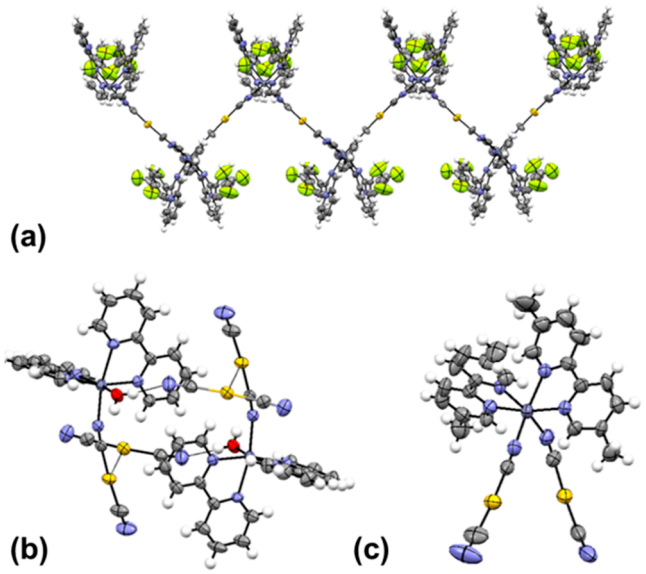

Figure 1. Representation of the main structural patterns in crystal structures of **1**–**8**: (a) 1D chain of Zn–Au fragments. (b) Dimeric or oligomeric basic unit of hydrogen and aurophilic bridged molecules and (c) molecular complex in **3** (ORTEP plot 40%).

predictable engineering of the crystalline state, we investigated the reaction of the $[Au(CN)_2]^-$ tecton with $[ZnL_2(H_2O)_{(0-1)}]^{2+}$ systems, where L is a chelating aromatic nitrogen donor ligand. The Zn^{II} ion has been chosen for the high solubility and stability of its chelated complexes in the presence of dicyanoaurate in a number of solvents, making possible the solution studies. The cationic fragment can only be coordinated by one or two other monodentate ligands. Indeed, the equilibrium characteristics of zinc-chelating ligand systems usually hinder the formation of the tris-chelate form.[15−18] By employing five differently substituted ligands, namely, L1 = 2,2′-bipyridine; L2 = 5,5′-dimethylbipyridine, L3 = 1-(2-pyridy)-3-(4-trifluoromethylphenyl)imidazo[1,5-*a*]-pyridine, L4 = 2-(2′-pyridyl)-1,8-naphthyridine, and L5 = 2,2′;6′,2″-terpyridine (Figure 2), selected for their different

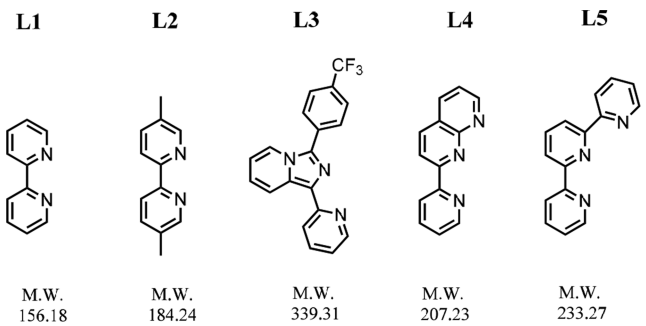

Figure 2. Structure of the employed organic ligands and their molecular weights.

steric (from the small L1 to the very bulky L3) and electronic properties (in L2, methyl donors make the ligand a stronger Lewis basis than L1, while L3 and L4 are weaker bases) as well as a number of possible coordination sites (two sites for L1, L2, and L3 and three sites for L4 and L5), we obtained nine mixed Zn–Au compounds: $\{Zn(L1)_2[(\mu\text{-}CN)Au(CN)](H_2O)\}[Au(CN)_2]$ (**1**), $\{[Zn(L2)_2[(\mu\text{-}CN)Au(CN)](H_2O)]\}[Au(CN)_2]$ (**2**), $\{[Zn(L2)_2[(\mu\text{-}CN)Au(CN)]_2\}(H_2O)$ (**3**), $\{Zn(L3)_2[Au(\mu\text{-}CN)_2]_2\}\cdot DMSO$ (**4**), $\{Zn(L3)_2[Au(\mu\text{-}CN)_2]\}_\infty[Au(CN)_2]\cdot DMF$ (**5**), $\{Zn(L4)[Au(\mu\text{-}CN)_2]_2\}_\infty\cdot ACN$ (**6**), $\{[Zn(L4)_2]_2[Au(\mu\text{-}CN)_2]\}[Au(CN)_2]_3$ (**7**), $\{Zn(L4)[(\mu\text{-}CN)Au(CN)]\}[Au(CN)_2]\cdot 3(H_2O)$ (**8**), and $[Zn(L5)_2][Au(CN)_2]_2$ (**9**).

The syntheses (see the Supporting Information for details) followed a common procedure: the zinc and the gold complex fragments were formed or dissolved in distinct ethanolic solutions and mixed after the establishment of the equilibrium (complete after 5 min of stirring at boiling temperature) with the stoichiometry:

$$2K[Au(CN)_2] + Zn(NO_3)_2\cdot 6H_2O + 2L_n \rightarrow \text{product(s)}$$

Crystallization occurred after slow evaporation of the resulting solutions or after redissolution in solvents with different polarities. We thoroughly characterized the resulting crystalline products using SC-XRD; Figure 1–3 report selected structural snapshots, while the representations of asymmetric units and used numerations for **1**–**9** can be found in the Supporting Information.

Structural and Vibrational Characterization in the Solid State. Crystals of **1** present a molecular complex with an octahedral Zn^{II} site surrounded by two cis-bonded L1 molecules, a water molecule and a dicyanometallate bonded through the bridging nitrogen site. This disposition around octahedral metal centers differs (as for all the product in this work) from the ethylendiammine derivatives $[Zn(en)_2(M(CN)_2)_2]$ (M = Au, Ag)[19−21] or analogous substituted ligands,[22,23] in which a trans disposition of chelating nitrogen donors is observed likely due to a smaller lateral steric hindrance for nonaromatic chelating ligands. The coordinated water has a central role in the architecture of interactions for **1**; both hydrogens participate to strong charge assisted hydrogen bonds with nitrogens of both the terminal cyanides, forming the dimeric architecture that can be seen in Figure 1b. The hydrogen interactions are directed toward fragments in the proximal dicyanometallate chains, dictating a staggered conformation in the aurophilic dimers formed by the cationic $\{Zn(L1)_2[(\mu\text{-}CN)Au(CN)](H_2O)\}^+$ fragment and a free dicyanoaurate (torsion angles between them is 72.51(5)°). These torsion angles between fragments involved in metallophilic interactions are similar to those founded in structurally and chemically analogous compounds with general formula $\{M(L)_2[M'(CN)_2](H_2O)\}[M'(CN)_2]$ (M = Zn, Mn, Ni, Cd; L = 1,10-phenantroline, 2,2′-bipyridine; M′ = Ag, Au).[24−27] At the same time, it is peculiar that this hydrogen bond seems to be strong enough to force a nonlinearity in the coordination of the cyanide to the Zn center, with a Zn-NC-Au angle of 158.68(7)°. The intrinsic proof of the strength of this interaction in the molecular geometry of **1** is that the anhydrous products reported in this work (**3**–**8**) do not present this strong distortion from linearity of the bimetallic Zn-CN-Au fragment (158.68(7)° for **1** with respect to 175.5(2)° for **3**, 176.8(3)° for **4**, 169.9(4)° for **5**, 166.5(3)° for **6**, 176.5(4)° for **7**, and 170.1(5)° for **8**). Moreover, the aurophilic interactions in **1** (d(Au1···Au2) = 3.267(2) Å, a value in the average of the interactions found for dicyanoaurate in CCDC) are supported not only by the Coulombic attraction between the positive $\{Zn(L1)_2[(\mu\text{-}CN)Au(CN)](H_2O)\}^+$ and the negative $[Au(CN)_2]^-$ fragments but also from this network of hydrogen bonds between a strong donor and acceptors (Figure S1a). The synergy among such strong interactions can

DOI: 10.1021/acs.inorgchem.9b00961
Inorg. Chem. 2020, 59, 203−213

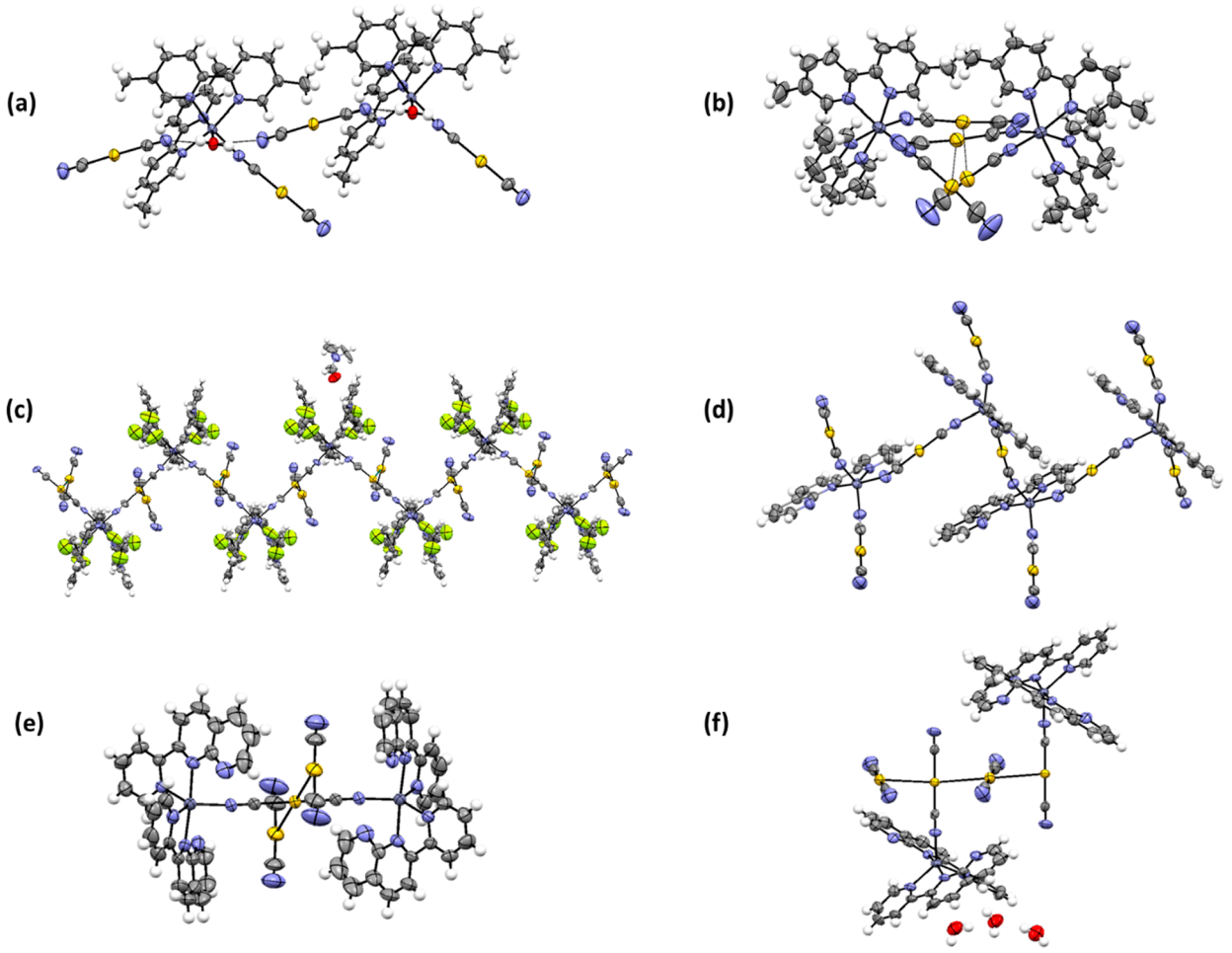

Figure 3. Structural pattern in the crystal structure of **2** (a), **3** (b), **5** (c), **6** (d), **7** (e), and **8** (f) (ORTEP plot 40%; color code: yellow, gold; dark gray, zinc; gray, carbon; cyan, nitrogen; red, oxygen; white, hydrogen; green, fluoride).

be the reason why it is difficult to resolubilize the solid sample after formation of the crystals also in strongly polar or coordinating solvents.

Similar to the previous system, in **2**, the asymmetric unit has a cationic $\{Zn(L2)_2[Au(CN)_2](H_2O)\}^+$ and an anionic $[Au(CN)_2]^-$ molecular fragment (Figure S3). The geometry around the zinc center is similar to that of previous species and does not seem influenced by the presence of two methyl groups far from the metal center. Despite this similarity at a molecular level, the methyl substitutions modify the arrangement of the two units in the crystal packing. The chain of Au(I)···Au(I) interactions becomes unfavorable probably because of steric factors, and the network is dominated by hydrogen bonding. In particular, the structure is connected by O−H···NC charge-assisted hydrogen bonds between the coordinated water donor and the dicyanometallate acceptor (Figure 3a) forming chains of the previously reported cationic and anionic fragments along *b* axes. Cyanometallates have been known for a long time as good hydrogen bond acceptors and have been used in crystal engineering for this peculiarity.[28,29] However, examples in which the crystal packing is directed only by this interaction are still rare: this can be due to the open environment around metal centers and the low steric hindrance of the cyanide ligand that make favorable the close location and interaction of other heavy atoms due to the similar strength of these two interactions.[30] In the simultaneous presence of aurophilicity and a hydrogen bond, the resulting architectures seem to confirm that these two interactions can be cooperative in the case of dicyanoaurate (and similar dicyanoargentate compounds).[31−33] However, the reported chain pattern is anomalous among the species that display a similar composition, and also for the only other complex of dicyanometallates presenting this ligand reported so far, $\{Cd(L)_2[Ag(CN)_2]_2\}$ (L= 5,5′-dimetyl-2,2′-bipyridine).[34] The minor tendency of Cd^{II} to be bonded to water in comparison with Zn^{II}, leaving a free coordination site and enabling the attachment of the bridging cyanide to the center of the complex, generates neutral molecules, whose disposition in the crystal packing is directed by the presence of a lattice water.

A behavior similar to the previously cited cadmium complex can be detected by changing the solvent from the polar protic ethanol (or DMF) to the less polar aprotic acetonitrile: the crystallization of **3** induces the water ligand to shift from the inner to the outer coordination sphere, while both the dicyanoaurates are linked to the octahedral zinc center of the complex, generating a neutral molecular complex. All the "V shaped" molecules are embraced (Figure 3b) to maximize the weak intermolecular aurophilic contacts between gold centers (d(Au1···Au2) = 3.400(3) Å), and these interactions are further stabilized by hydrogen bonds derived from the interstitial water molecule.

DOI: 10.1021/acs.inorgchem.9b00961
Inorg. Chem. 2020, 59, 203−213

The big steric hindrance and the presence of a DMSO lattice solvent molecule prevent the formation of aurophilic interactions in the molecular environment of the 0-D complex **4** (Figure S11) obtained from L3. The molecular structure is identical to complex **3**. The two noncoordinating substituted phenyl rings in the coordinated aromatic ligands are coplanar to the pyridine ring of the other coordinated molecule, interacting with the previous one with an intramolecular $\pi\cdots\pi$ stacking and lowering the internal steric hindrance, as observed in other similar bischelated complexes of this family of ligands.[35] The crystal packing is dominated by coupling between dipoles of organic fragments, with the disordered DMSO molecules in a region between the envelope of the aromatic rings of a molecule and the dicyanoaurate arms of the other frontal molecules.

It is interesting to compare the thermal stability of this purely molecular system to the hydrogen-bond-stabilized **2** and the aurophilicity and hydrogen-bond-stabilized **1**. TGA analysis demonstrates a clear stabilization due to the two directional interactions, with a degradation temperature of 180 °C for **4**, 220 °C for **2**, and 240 °C for **1** (see Figure S15). The latter compound was demonstrated to be the most robust notwithstanding the presence of a coordinated water.

Changing the crystallization solvent to DMF and maintaining the previous composition, it is possible to observe a drastic change of the crystal packing in product **5**: also in this case, both vacant sites of the zinc octahedron are occupied by cyanides, but dicyanoaurate is involved in a 1D infinite wavy cationic coordination polymer. The charge is neutralized by the presence of a noncoordinating $[Au(CN)_2]^-$ anion that strongly interacts with gold centers of the chain (d(Au1···Au2) = 3.234(3) Å, see Figure 3c). Similar behavior has been reported in the case of the Cu^{II}–Ag^{I} derivative of L1 $\{Cu(L1)_2[Ag(CN)_2]\}_\infty[Ag(CN)_2]\cdot(H_2O)$.[36]

Compound **6**, crystallized from acetonitrile as yellow-orange prisms, has a different zinc environment compared to the other members of this family, due to the complexation of only one chelated ligand: this is a true 1D coordination polymer, as with **5**, with three dicyanoaurate ligands bonded to trigonal bipyramidal zinc centers and forming a wavy chain along the [010] direction (Figure 3d). One of the three dicyanoaurates, however, is not bridging and forms an ancillary arm of the chain along [001] directions. This terminal ligand interacts with lateral chains by means of strong aurophilic interactions (d(Au1···Au2) = 3.207(3) Å) by forming 2D layers in the (001) planes (Figure S12). The L4 ligand coordinates Zn^{II} centers as a monochelated ligand from the pyridine substituent for the small bite of naphtyridinic nitrogens (the same behavior has been observed in all other nonmetallophilic d^{10} centers).[37]

From the same acetonitrile solution, yellowish crystals of compound **7** have been obtained. In the molecular complex, the zinc centers are coordinated by two nonequivalent L4s and a cyanide of a dicyanoaurate moiety, forming a regular trigonal bipyramid coordination polyhedron. Four different fragments can be detected: a cationic fragment where a dicyanoaurate bridges between two zinc centers, two ordered uncoordinated dicyanoaurates, and a disordered free dicyanoaurate. In the packing, it is possible to observe rows of gold centers similar to **1**, but the steric hindrance due to asymmetric naphtalenic rings suspends the chain of metallophilic interactions and makes possible the formation of a strong trimeric aurophilic architecture (d(Au1···Au2) = 3.146 Å, see Figure 3e). In the trimer, two lateral anionic $[Au(CN)_2]^-$ molecules are almost perpendicular to the central tricationic structure (98.70(5)° between the bridging cyanide and the lateral terminal ones) and the terminal ligands weakly interact with the C–H of nearby aromatic rings. The disordered dicyanoaurate molecule lays in two positions around an inversion center in a region surrounded by aromatic rings and does not participate in any strong directional interactions.

Changing the solvent to polar protic ethanol and maintaining the same 1:2 Zn/L4 ratio, an aurophilic chain of cationic molecular $\{Zn(L4)_2[(\mu\text{-}CN)Au(CN)]\}^+$ and anionic $[Au(CN)_2]^-$ fragments can be observed in compound **8**. This disposition is more similar to the case of **1** than to the other crystal packing obtained in the case of L4 systems, demonstrating the structural analogy of L4 with L1. It is possible to observe a monocationic fragment $\{Zn(L4)_2[(\mu\text{-}CN)Au(CN)]\}^+$ presenting a trigonal bipyramidal zinc coordination center and a noncoordinated dicyanoaurate anion interacting with strong aurophilic contacts with the first center (d(Au1···Au2) = 3.166(2) Å and d(Au2···Au3) = 3.189(2) Å). Despite the similarity with product **1**, the absence of a water molecule as a hydrogen bond tecton makes the geometry of the cationic fragment more linear (angle Zn1–CN–Au1 of 171°) and the disposition of anionic and cationic fragments along the aurophilic interaction more perpendicular with respect to **1** (torsion angle of cyanides with respect to the Au–Au axis of 71.5(7)°) and more omogeneous, forming a continuous chain of gold centers along b axes (Figure 3f).

The last complex (**9**) was prepared with the tridentate L5 molecule to confirm the necessity of bidentate chelating ligands to obtain Zn–Au molecular aggregates. In **9**, the zinc distorted octahedral molecular centers are surrounded by nitrogen from two L5 ligands, and anionic dicyanoaurates cocrystallize separately to form aurophilic dimers surrounded by aromatic rings (d(Au1···Au2)= 3.149(3) Å, see Figure S13).

For all the solid products, MIR, FIR, and Raman spectra provided an important support in understanding the structure on the basis of the cyanide moieties. The ν(CN) bands for **1**–**9**, $K[Au(CN)_2]$, and $\{Zn(phen)_2[Au(CN)_2]\}[Au(CN)_2]\cdot$EtOH (phen = 1,10-phenantroline),[24] considered due to its similarity to **1**, can be found in Table S26, while representative FIR spectra are reported in Figure S14. All the characterized compounds present a signal near 2140 cm^{-1} in MIR spectra and at 2160 cm^{-1} in Raman spectra, similar to that of the potassium dicyanoaurate salt and of dicyanoaurate in solution,[38] characteristic of terminal cyanide groups.[39] The blue-shifted bands (relative to free $[Au(CN)_2]^-$) observed for all the other reported compounds (unless complex **9**) are characteristic of bridging cyanide, with the shift relative to the strength of the bond,[40] or of hydrogen bonding acceptor cyanides. In the FIR region, the strongest signal for all the complexes is the ν(Au–C) mode that can be found near 442 cm^{-1} or blue-shifted with respect to free dicyanoaurate and the two bending modes of this linear molecule near 176 and 123 cm^{-1}. The ν(Zn–N) mode, however, is visible near 400 cm^{-1} in the cases of **1** and **2**, as reported in the literature for bipyridine complexes, while it is very weak in phenanthroline and other complexes.[41−44]

Solution Studies. We will later decipher the general trends yielding to the observed solid-state configurations, based on the insight reported herein about the solution chemistry of these systems. For all the synthesized compounds, the solution behavior was analyzed before and after the addition of dicyanoaurate with a number of techniques, to check the

DOI: 10.1021/acs.inorgchem.9b00961
Inorg. Chem. 2020, 59, 203−213

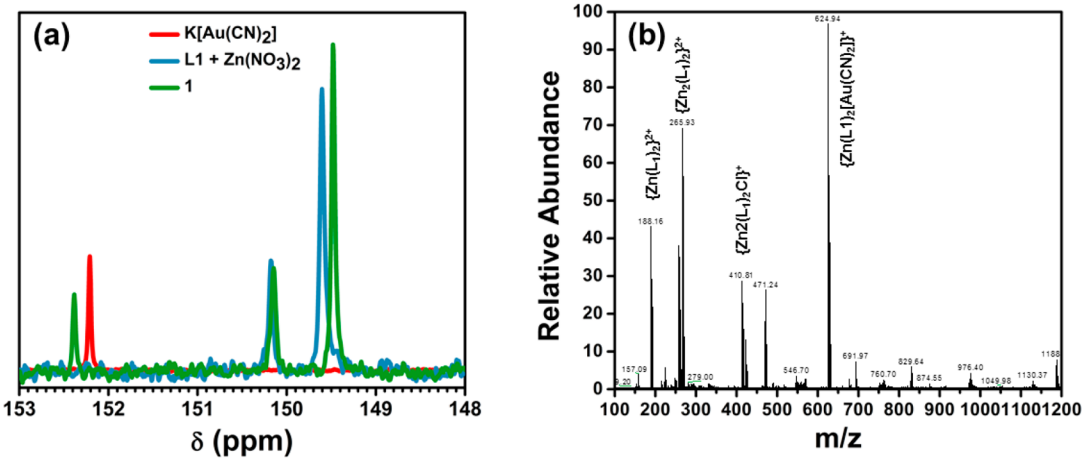

Figure 4. (a) Superimposition of ^{13}C NMR spectra of $K[Au(CN)_2]$, L1 with $Zn(NO_3)_2$ (2:1 ratio), and **1** in saturated methanolic solutions and (b) ESI-MS spectrum of $ZnCl_2$/L1/$K[Au(CN)_2]$ (1:2:2 ratio) ternary mixture in ethanolic solution (10^{-4} M).

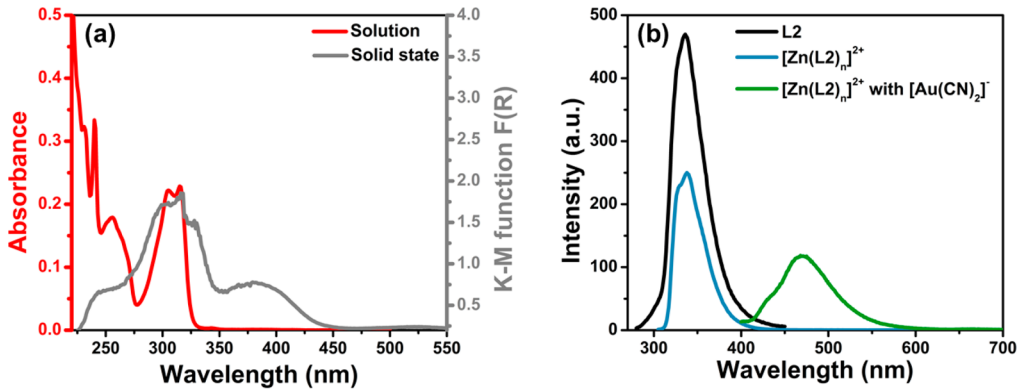

Figure 5. (a) Solution absorbance spectrum of $[Zn(L2)_n]^{2+}$ with $[Au(CN)_2]^-$ in ethanolic solution (96%) at 10^{-4} M and solid state diffuse reflectance of crystalline powder of **2** with silica 1:20. (b) Emission spectra of L2, $[Zn(L2)_n]^{2+}$ (10^{-4} M) and $[Zn(L2)_n]^{2+}$ with $[Au(CN)_2]^-$ (10^{-3} M) in ethanolic solution (96%).

equilibrium effects and the presence of self-assembly. ^{13}C and ^1H NMR, absorption and emission UV−vis spectroscopy, electro spray ionization-mass spectrometry (ESI-MS), and X-ray absorption spectroscopy (XAS) at both the Au L_3-edge and Zn K-edge were applied to clarify the different aspects of solution behavior and characterize both structurally and spectroscopically the resulting complexes.

Solution Behavior of Zn/L Systems. When L1−L4 are added to an ethanolic solution of a Zn^{II} salt in a 2:1 L/Zn ratio, the complexation equilibria occur. These phenomena can be effectively monitored by absorption and emission UV−vis spectroscopy, as well as ESI-MS. As detailed in the SI, electronic absorption spectra of solutions obtained mixing Zn^{II} and Ln (n = 1, 2, and 4) ligands show a red shift of 20 nm in comparison with the absorption maxima in solution of the free ligands. A stronger ligand-dependent effect can be observed in the emission spectra obtained from a 230 to 300 nm excitation wavelength: L1 shows a strong bathochromic shift of 15 nm with respect to the emission of the free ligand. L2 during the complexation does not show a shift compared to the 336 nm maximum of the free ligand, while L3 and L4 show a hypsochromic shift of 20 nm. The same phenomenon can be observed by comparing ^{13}C and ^1H NMR spectra of free L1 with those of the complexed ligand. To study in detail the speciation in these solutions, ESI-MS spectra of 10^{-5} M ethanolic solutions of ZnX_2/L1 (X = NO_3^-, Cl^-) in a 1:3 ratio were collected. The ESI-MS results are a good approximation of the behavior of solution species and have often been used to study the speciation of coordination compounds, although in some cases, the possibility of some modifications occurring in the passage from the condensed to gas phase cannot be ruled out during the ESI process.[45−47] The chemistry of the two systems is similar, but the species show some differences due to the different bonding strengths of nitrate and chloride. It is important to observe that in solution both mono- and bis-chelated species are present, with a lower presence of bare $[Zn(L)_n]^{2+}$ in the case of chloride. Moreover, the trischelated $[Zn(L)_3]^{2+}$ complex can be detected only in the nitrate solution and is absent in the chloride solution, suggesting a stronger anion complexation in the latter case.

Solution behavior of Zn/L/$[Au(CN)_2]^-$ Systems. The addition of dicyanoaurate to these equilibria has been studied to check the presence of aggregation between the Au^I and the Zn^{II} fragments. Indirect proofs of this phenomenon have been obtained from electronic and NMR spectra. UV−vis absorption spectroscopy apparently suggests the absence of any kind of interaction: the mixture of the two compounds, in all cases, exhibits a spectrum corresponding to the sum of those individually stemming from zinc complexes and dicyanoaurate (see Table S30 in SI).[48] However, two different clues point to the presence of another weaker absorption at 380 nm; first, the solid state absorption spectra of all the solid

DOI: 10.1021/acs.inorgchem.9b00961
Inorg. Chem. 2020, 59, 203−213

samples, although very similar to those in solution, show a large band in the visible region (Figure 5a for the explicit case of the solid spectrum of **2** compared to the solution of the corresponding complex) that does not seem to be present in solution. Moreover, TD-DFT calculations on the cationic fragment $\{Zn(L)_2[(\mu\text{-}CN)Au(CN)](H_2O)\}^+$ extracted from crystal structures predict an electronic transition in this region linked to the mixed metal fragment (see Figure S38). This transition seems to be a charge transfer in nature, with a dicyanoaurate-localized HOMO and a zinc centered LUMO, although the nature of this transition has to be analyzed in more detail in future work. In addition, we found that the ternary mixtures under deoxygenated conditions show an intense emission at about 460−470 nm, by exciting at about 380 nm at a 1 mM concentration, as observable in Figure 5b for the case of the L2 system in ethanolic solution. However, for the observed transition a pure charge transfer localized on dicyanoaurate can be unequivocally rejected because this kind of transition is at a lower wavelength (see Table S28) and not emissive at room temperature in the analogous range of concentrations.[48,49] This oxygen-dependent emission implies the formation of an emissive adduct between $[Zn(L)_n]^{2+}$ and $[Au(CN)_2]^-$. Similar results have also been obtained in the cases of $[Zn(L1)_n]^{2+}$, $[Zn(L3)_n]^{2+}$, and $[Zn(L4)_n]^{2+}$ in the presence of dicyanoaurate under the same concentrations (see Tables S29 and S30). It is important to remark that the concentration employed to observe such emission is 100 times lower than that previously reported for the formation of luminescent aurophilic oligomers. Therefore, the concentration range adopted in this study excludes the emission also from these entities.[49,50] Further evidence of the interaction between $[Zn(L)_n]^{2+}$ and $[Au(CN)_2]^-$ in solution can be deduced from the analysis of the excitation spectra of the mixtures (see SI, part 4). In general, the excitation spectra are superimposable to the corresponding absorbance profile, if recorded at the emission value of $[Zn(L)_n]^{2+}$ species (230−300 nm); this implies the presence of a single emitter in solution. Nonetheless, the excitation spectra of the ternary degassed solutions, collected at the emission value of the $[Zn(L)_n]^{2+}$-$[Au(CN)_2]^-$ adducts, show clearly an intense peak in the 320−400 nm range. This observation is particularly significant for L1 and L2 because the corresponding $[Zn(L)_n]^{2+}$ complexes do not show any absorption beyond 320 nm. Another surprising observation concerns L3; in this particular case, the emissions of the free ligand, the $[Zn(L)_n]^{2+}$, and the $[Zn(L)_n]^{2+}$−$[Au(CN)_2]^-$ species appear in the same range. However, the excitation spectrum obtained from the ternary mixture under deoxygenated conditions reveals the peculiar peak of the dicyanoaurate anion at 240 nm, which means that the emissive species include a dicyanoaurate moiety (see Figure S32). The results have been confirmed by an NMR study in solution of the ternary mixture of L1. The addition of a stoichiometric amount of dicyanoaurate to the solution has a limited but evident effect on both ^1H and ^{13}C signals of the complexes (reported in SI Figures S16, S17). In particular, the singlets at 149.5 (C6 of L1) and 152.4 (dicyanoaurate) ppm in the ^{13}C NMR spectrum of the mixture (Figure 4a) fall at lower and higher frequencies, respectively, if compared to the spectra of pure $[Zn(L1)_n]^{2+}$ and dicyanoaurate. This behavior is compatible with the coordination of the dicyanoaurate to the zinc metal center, causing the shielding of the C6 of the L1 ligand and the concomitant deshielding of the carbon of the cyanide ligand. An analogous effect can be observed in the ^1H NMR spectra in Figure S16, where the signal at 8.81 ppm of the $[Zn(L1)_n]^{2+}$ complexes shifts to higher frequencies after the addiction of dicyanoaurate.

To obtain more detailed information on the speciation in the ternary mixtures, ESI-MS has been applied to all the families of ligands. When the ESI-MS of the three ternary mixtures (1:2:2 ratio) $ZnCl_2/K[Au(CN)_2]/L_n$ (n = 1, 3, and 4) are compared, some general considerations may be drawn. First, the different systems display a very similar solution chemistry, since a family of four ions ($[ZnL_2]^{2+}$, $[ZnLCl]^+$, $[ZnL_2Cl]^+$, and $\{ZnL_2[Au(CN)_2]\}^+$) is present in all the mixtures and represents the larger number of signals in the spectra. However, when the relative abundance of these ions is compared with those of the other signals, it becomes evident that they display the highest abundance in the L1 system (representative case reported in Figure 4b), followed by the L3 and the L4 systems. This order may be related to the tendency of the three different N-donor ligand families to coordinate Zn^{II}. Second, all the systems display the $\{ZnL_2[(\mu\text{-}CN)Au(CN)]\}^+$ ion, which corresponds to the species detected in almost all the solid products, except for the absence of a coordinating water molecule. When subjected to MS/MS experiments, these bimetallic ion species displayed very similar fragmentation patterns: the main product is the $\{ZnL(CN)\}^+$ ion, which is formed through both parallel and consecutive L and AuCN losses in the L1 system and exclusively by a simultaneous loss of the two neutral moieties in the other two cases. Importantly, this fragmentation pattern confirms that the Zn−Au species are not a weak interacting charge couple but a coordination bonded complex through the cyanide as in the solid state.

It is remarkable, however, that no water containing ion complexes (similar to those found in **1** and **2** crystal structures) were detected, apart from the products of MS/MS experiments, where they are produced in low abundance (e.g., the $\{Zn(L1)(H_2O)[Au(CN)_2]\}^+$ ion). This effect is curious, because the water in the reported cases is strongly bonded to Zn^{II} in the solid state (dehydration temperature for **1** and **2** measured with TGA: 180 and 120 °C, see Table S27), and its absence can be related to the passage to gas phase.

Dimeric cluster species are observed in the diluted solution of Zn^{II} (1.0×10^{-5} M)/L3/$[Au(CN)_2]^+$ at a 1:2:1 molar ratio, despite L3's basicity and despite L3 being the bulkiest among the considered ligands: the $\{Zn_2L_2[Au(CN)_2]_2\}^{2+}$ (m/z 653) and the $\{Zn_2L_3[Au(CN)_2]_2\}^{2+}$ (m/z 822) ions. An important contribution of the dimeric $\{Zn_2L_2[Au(CN)_2]_2\}^{2+}$ species has been observed, similarly, in the L4 solution at a Zn^{II} 1.0×10^{-5} M concentration. These fragments are not detected in the L1 system; however, given the similarity observed in the solid state phase between the L1 (compound **1**) and L4 (compound **8**) systems, we also investigated the L1 system at higher solution concentrations in the search for heavier clusters.

When the $ZnCl_2$ (1×10^{-3} M)/L1/$K[Au(CN)_2]$ 1:2:1 mixture was studied, it was observed that the relative abundance of the $\{Zn(L1)_2[Au(CN)_2]\}^+$ cluster further increases, and new signals attributed to the following cluster species appear: $[Zn_2(L1)_2[Au(CN)_2]_2\}^{2+}$ (main peak at m/z 471), $\{Zn_2(L1)_3[Au(CN)_2]_2\}^{2+}$ (m/z = 549), $\{Zn_3(L1)_3(Au(CN)_2)_4\}^{2+}$ (m/z = 830), and $\{Zn_4(L1)_4[Au(CN)_2]_6\}^{2+}$ (m/z = 1191) (Figure S35a). Since water is present in none of these ions, hydrogen bonds between the H atoms of the water molecule linked to one Zn center and one of the N atoms of the dicyanoaurate group of another monomer can be safely

DOI: 10.1021/acs.inorgchem.9b00961
Inorg. Chem. 2020, 59, 203−213

ruled out, and formation of these species is likely due to aurophilic Au−Au interactions and/or to dicyanoaurate anions bridging two zinc centers, as can be detected in some solid products. However, CID experiments performed on the $\{Zn_3(L1)_3[Au(CN)_2]_4\}^{2+}$ (m/z 830), and $\{Zn_4(L1)_4[Au(CN)_2]\}_6^{2+}$ (m/z 1191) ions did not provide insights about their connectivity. In fact, for the former ion, a simple loss of one L1 molecule is observed, while, for the other ion, consecutive losses of two L1 molecules occur, followed by the addition of two water molecules, yielding the $\{Zn_4(L1)_2(H_2O)_2[Au(CN)_2]_6\}^{2+}$ ion.

Structural Characterization of Grow Unit in Solution by XAS. Aiming at a direct determination of the solution-phase structure of complex **1** ($\{Zn(L1)_2[(\mu\text{-}(CN)Au(CN)]\text{-}(H_2O)\}[Au(CN)_2]$), we have collected XAS data at both the Au L_3-edge and Zn K-edge. Exploiting the element selectivity of the technique and the possibility to operate under high-dilution conditions with fluorescence-mode detection, we have refined the local structure of Au and Zn centers in a 5×10^{-4} M ethanolic solution of **1**. The selected working concentration was low enough to safely prevent crystallization over the 6−8 h period required to obtain quantitatively analyzable EXAFS spectra. Figure 6 reports an overview of the collected XAS data, providing a direct comparison of the XANES and EXAFS spectra of **1** in solution and in the solid state. At each absorption edge, the XANES spectra of the investigated complex are further compared to the ones obtained for relevant model compounds in the solid state, i.e., $K[Au(CN)_2]$ and complex **9** ($[Zn(L5)_2][Au(CN)_2]_2$, L5 = 2,2′;6′,2″-terpyridine), chosen for the octahedral nitrogen environment for Zn^{II} in **9** and for aurophilic interaction between linear AuI complexes in $K[Au(CN)_2]$, to guide the interpretation of the observed spectroscopic features

For both metal centers, the XANES spectra in solution and in the solid state are virtually indistinguishable and very similar to the ones of the model compounds reported here and in previous literature.[51,52] Thus, an unaltered oxidation state (Au^{I}, Zn^{II}) and a similar local coordination geometry is confirmed both in solution and in the solid state. A qualitative comparison of the correspondent FT-EXAFS also reveals strong similarities, further corroborating the fact that the same metal coordination environment as characterized in the solid state is conserved in solution at least up to the second coordination sphere of the cations.

Nonetheless, especially in the Au L_3-edge, we note differences in the EXAFS signal in the 2−3 Å region. In particular, the intensity of the maximum peaking at ca. 2.5 Å in the phase-uncorrected spectra significantly diminishes in the solid-state spectrum with respect to the solution-phase one.

Driven by these qualitative insights, we have performed EXAFS fitting of the solution-phase spectra of **1** reported in Figure 6c,d. Capitalizing on the thorough structural characterization obtained in the solid state, as well as on the other experimental evidence reported in this work, we have adopted the XRD model of the $\{Zn(L1)_2[Au(CN)_2](H_2O)\}^{+}$ unit as an initial guess in EXAFS refinements at both the Au L_3- and Zn K-edge (see Figure 7a). On the basis of previous studies, we do not expect aurophilic interaction in the solution phase in the concentration range adopted in the EXAFS experiments, as has been considered for emission behavior.[49,50] Thus, in the EXAFS analysis of **1** in ethanolic solution, we only considered the presence of virtually isolated $[Au(CN)_2]$ and $\{Zn(L1)_2[(\mu\text{-}CN)Au(CN)](H_2O)\}^{+}$ units, in a 1:1 ratio. The fitting results

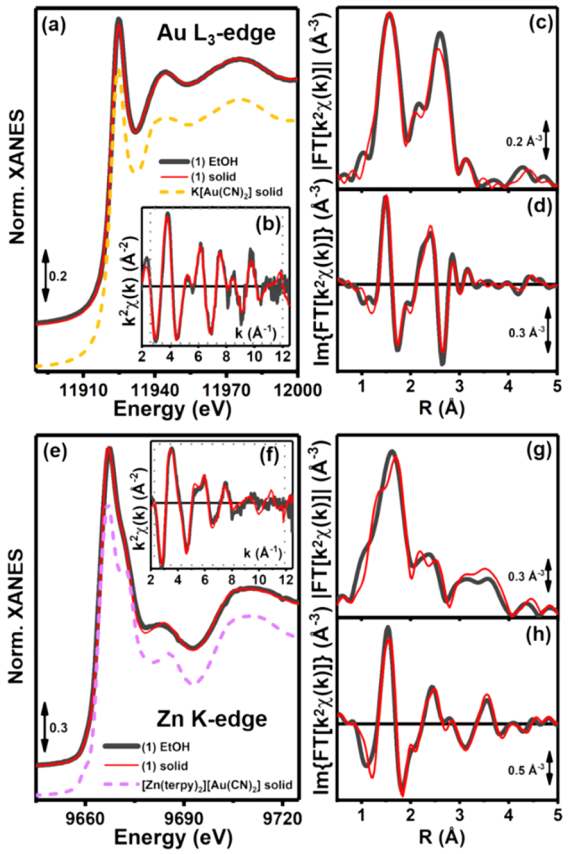

Figure 6. (a) Au L_3-edge XANES of **1** in ethanolic solution and in the solid state. The XANES of the $K[Au(CN)_2]$ reference compound, measured in the solid state, is also reported, vertically translated for the sake of clarity. (b) $k^2\chi(k)$ EXAFS spectra of **1** in ethanolic solution and in the solid state. The k range employed for the FT is highlighted by a dotted gray box. (c, d) Phase-uncorrected (c) modulus and (d) imaginary part of the FT-EXAFS spectra for **1** in ethanolic solution and in the solid state. (e) As part a but reporting Zn K-edge XANES data for **1**, and the XANES spectrum of complex **9**, measured in the solid state, vertically translated for the sake of clarity. (f−h) As parts (b−d), respectively, but reporting EXAFS data collected for 1 at the Zn K-edge.

reported below, in combination with the EXAFS characterization of the model compounds $K[Au(CN)_2]$ and complex **9**, will then serve to validate our initial hypotheses.

Figure 7b−e reports an overview on the EXAFS fitting results at both the investigated absorption edges. It is clear that the adopted structural model ensures a good reproduction of the experimental signal (R factor < 1.4% at both edges), together with physically meaningful values of all the guessed parameters (see Table S32). Hence, the fitting results support the validity of the adopted structural model, while allowing the assignment of the various contributions to the EXAFS signal.

As illustrated in Figure 7b,c, the Au L_3-edge EXAFS of **1** in ethanolic solution is dominated by two maxima peaking at ca. 1.5 and 2.8 Å in the phase-uncorrected spectrum. As expected, the first maximum stems from SS paths involving the first-shell $\mathbf{C1}_{AuL}$ atoms of the two cyanide ligands (see Figure 6a for atom labeling code). The origin of the second maximum is more peculiar. Indeed, whereas we observe a minor contribution from the SS involving the second-shell $\mathbf{N2}_{AuL}$ atoms, the main contribution to the EXAFS signal arises from a series of unusually intense collinear MS paths involving the

DOI: 10.1021/acs.inorgchem.9b00961
Inorg. Chem. 2020, 59, 203−213

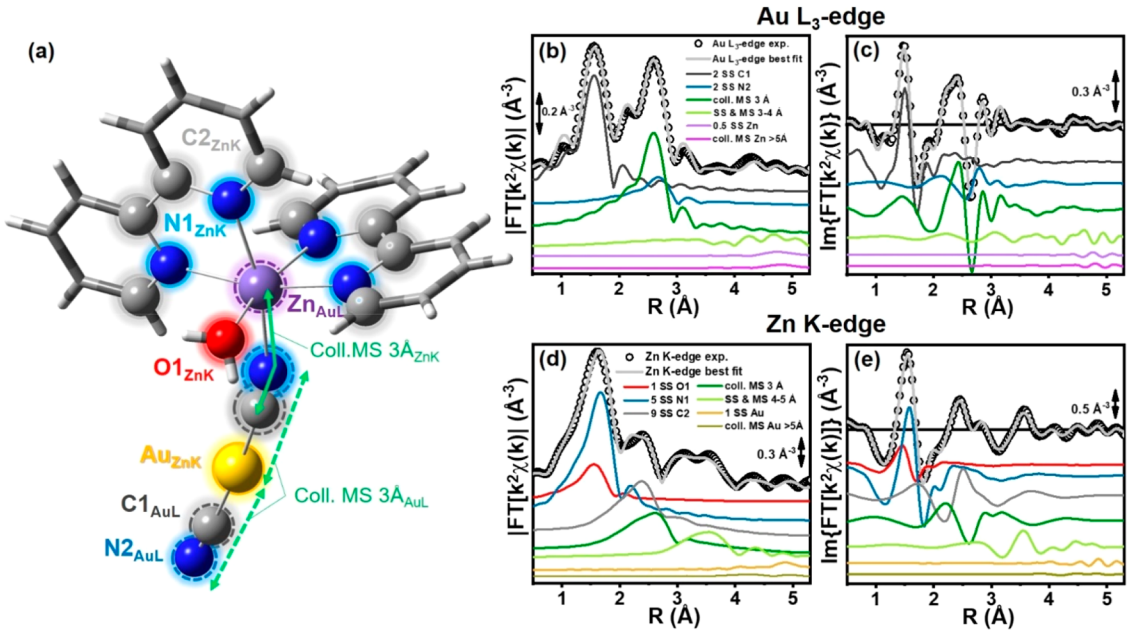

Figure 7. (a) Structural model of the $\{Zn(L1)_2[(\mu\text{-}CN)Au(CN)](H_2O)\}^+$ unit obtained from XRD refinement of **1** in the solid state. Atom color code as follows: Au, yellow; Zn, violet, H, white; N, blue; C, gray; O, red. The atoms located in the first and in the second coordination shells of the metal centers are shown in ball and stick mode, while the atomic neighbors located at higher distances are depicted in stick-only mode. Colored circles and corresponding labels denote the different shells of scattering atoms employed for EXAFS fitting (full and dashed circles refer to the local environment of Zn and Au, respectively). The atoms involved in the unusually intense collinear MS contributions observed for this system are also highlighted by green arrows. (b, c) Comparison between experimental and best fit EXAFS spectra collected at the Au L_3-edge (magnitude and imaginary parts in panels b and c, respectively) for **1** in ethanolic solution. The principal contributions to the EXAFS signal are also reported, using the same color code as in part a and vertically translated for the sake of clarity. (d, e) As parts b and c but for data collected at the Zn K-edge

$\mathbf{C1}_{\mathbf{AuL}}$ and $\mathbf{N2}_{\mathbf{AuL}}$ of the cyanides. While collinear MS paths are known to commonly exhibit a higher amplitude than other kinds of MS, the present case represents an iconic example.[53]

In addition, EXAFS confirmed the absence of Au···Au interactions in the solution phase at the employed concentration of 5×10^{-4} M. On the basis of solid-state structural analysis of **1**, these result in Au···Au distances falling in the 3.2−3.6 Å range, which should perturb the EXAFS signal in the second-shell region. The excellent fitting reached in the absence of these additional scattering contributions indirectly supports the lack of metallophilic interactions in the solution phase under our experimental conditions.

We further explored this point by comparatively analyzing the Au L_3-edge EXAFS spectra of **1** and of $K[Au(CN)_2]$ in both ethanolic solution and in the solid state (Figure S36). The subtle differences observed in the 2−3 Å region between solution phase and solid state can be safely connected with additional Au···Au scattering paths in both the solid-state samples (refined at ca. 3.14 and 3.48 ± 0.06 Å and at 3.16 and 3.52 ± 0.06 Å for **1** and $K[Au(CN)_2]$, respectively).

Importantly, we were able to locate the $\mathbf{Zn}_{\mathbf{AuL}}$ center, best-fitted at 5.15 ± 0.06 Å from the Au center with a fixed coordination number of 0.5 (accounting for 50% of Au sites occurring as "isolated" $[Au(CN)_2]^-$ units). Not surprising, the long-range Au−Zn_{AuL} SS gives a rather weak contribution to the overall signal (purple line in Figure 7b,c). Nonetheless, it is still successfully refined in the fit, with an optimized DW of $\sigma^2_{Zn} = 0.005 \pm 0.002$ Å^2, in line with the expectation values for a high-Z scatterer at >5 Å from the absorber. In the same R-space region, the contribution from MS paths arising from the close-to-linear arrangement of the Au−C−N−Zn moiety is also appreciable (pink line in Figure 7b,c), with an amplitude comparable with the Au−Zn_{AuL} SS path.

This is a first line of evidence supporting the presence of preorganized $\{Zn(L1)_2[(\mu\text{-}CN)Au(CN)](H_2O)\}^+$ units in diluted solutions of **1**. Further support comes from fitting of the Zn K-edge spectrum of **1** in EtOH (Figure 7d,e, main text). Also in this case, the adopted structural model ensured a very good reproduction of the experimental spectrum. The first-shell region in the EXAFS is properly fitted by two subshells of low-Z atomic neighbors, including a shorter $\mathbf{O1}_{\mathbf{ZnK}}$ contribution at 2.01 ± 0.02 Å (plausibly from a tightly coordinated H_2O ligand also identified in the solid state) and a longer $\mathbf{N1}_{\mathbf{ZnK}}$ subshell, refined at $<R_{N1}>$ 2.16 ± 0.06 (Å). The latter comprises four N atoms belonging to the L1 ligands as well as the N atom of the dicyanide, which cannot be discriminated by EXAFS. Importantly, EXAFS supports a 6-fold coordinated Zn center also in the solution phase. In this respect, the test fits performed excluding the $\mathbf{O1}_{\mathbf{ZnK}}$ contribution resulted in an unphysically high S_0^2 value of 1.4 ± 0.1,or in a poor fitting quality once S_0^2 is constrained to the ideal value of 1 (R factor = 0.02432, more than doubled with respect to the value of 0.01175 obtained employing the 6-fold coordinated model in Figure 7a).

The second-shell region in the Zn K-edge EXAFS is particularly insightful, especially in the view of assessing the presence of mixed-metal units in diluted solutions of **1**. Indeed, the $\{Zn(L1)_2[(\mu\text{-}CN)Au(CN)](H_2O)\}^+$ unit displays an almost linear connectivity between the two metal centers through the cyanide group, with a Zn−C−N angle of ca. 163° (from XRD refinement in the solid state). Such a characteristic bond geometry translates into the presence of high-amplitude collinear MS paths also in the Zn K-edge EXAFS, finger-

DOI: 10.1021/acs.inorgchem.9b00961
Inorg. Chem. 2020, 59, 203−213

printing the presence of collinear Au···Zn units also in the solution phase. These scattering contributions (coll. MS $3Å_{ZnK}$, dark green line in Figure 7d,e, main text) are indispensable to adequately fit the experimental spectrum. Being in partial antiphase with the SS paths involving the $C2_{ZnK}$ atoms (gray line in Figure 7d,e, main text), they reshape the spectrum in the 2.8−4.0 Å region. These MS contributions allowed us to account for the pronounced intensity decrease of the second-shell peak in **1** with respect to what is observed in the EXAFS of the solid-state complex **9**, together with the slightly lower coordination number (N_{C2} = 9 and 12 in complex **1** and in complex **9**, respectively (Figure S37).

Finally, as previously discussed for Au L_3-edge EXAFS analysis, also at the Zn K-edge, we were able to successfully include, in the fitting model, the weak contribution from the distant Au_{ZnK} scatterer (yellow lines in Figure 7d,e), refined at 5.05 ± 0.05 Å from the Zn center (compatible with the AuZn distance obtained from the analysis of Au L_3-edge data within the respective fitting errors, see Table S32). Also in this case, a series of rather intense MSs arises around 5 Å due to the quasi-linear Zn−N−C−Au configuration. Nonetheless, also due to antiphase effects among these paths, in this case, the global contribution (dark yellow line in Figure 7d,e) is less evident with respect to what was observed at the Au L_3-edge.

Discussion: Bridging Solution and Solid-State in Dicyanoaurate Structural Chemistry. By demonstrating the supramolecular aggregation in solution, the formation of the bimetallic growth unit, and the oligomerization at different concentrations, it is possible to analyze the solid-state structures of **1**−**9**, recognizing the patterns that arise from the association of these fundamental building units. For most of the structures, the cationic growth unit is clearly maintained. In the cases of **1**, **2**, **8**, and **9** it interacts with the anionic free dicyanoaurate fragment through aurophilicity (and hydrogen bonding in the presence of the water ligand, see Figure 1b). Conversely, for compounds **5** and **6**, aggregation by coordination bonds to form head-to-tail cationic chains occurs (Figure 1a), and this is supported by the detection of oligomeric species also at low concentrations by ESI-MS. This behavior has usually been observed in the most polar crystallization solvent. When lower polarity solvents were used, the attachment of anionic $[Au(CN)_2]^-$ fragments to the Zn^{II} occurred, forming neutral molecular complexes (structures of **3** and **4**, Figure 1c). Comparing the ESI-MS spectra of the three ternary mixtures (analyzed at the same concentration), it turns out that the L3 and L4 systems display the highest nuclearity among the three systems. This is in agreement with the solid-state crystallography results, where polymeric structures are observed for L3 and L4 ligands. These findings allows us to confidently establish a direct connection between solution and solid state results, which also finds support in a previous study by Chu et al.[54] on a similar system concerning the dicyanoaurate ion. In this report, a polymeric solid state structure is obtained where nickel(II) units coordinated by tris(2-aminoethyl)amine (tren) ligands are linked by $Au(CN)_2^-$ to form infinite zigzag chains. ESI-MS investigation of the solute dissolved in a water/methanol mixture revealed the formation of $[Ni(tren)]_n[Au(CN)_2]_{2n-1}^+$ and $[Ni(tren)]_n[Au(CN)_2]_{2n-2}^{2+}$ ions, whose structure was described by the authors, on the basis of solid state XRD evidence, in terms of an oligomeric cation associated with one or more dicyanoaurate units. The former ion family resembles the $\{Zn_2L_2[Au(CN)_2]_2\}^{2+}$ species observed by us in the L3 and L4 systems (and for L1 at higher concentrations), which may be considered the precursors for polymerization in the solid phase. However, a direct connection between solution and solid phases could not be established for the L1 system, since the solution species do not contain coordinated water, and hence formation of solution olygomers takes place in a different way with respect to the solid phase, where hydrogen bonds play an important role. Moreover, ESI-MS analysis requires dissolution of samples in polar solvents, and hence we could not investigate the effects of less polar solvents on aggregation mechanisms, which were instead appreciated in the solid phase, where different solvents lead to different structures with the same ligand (compare compounds **4** and **5**). Therefore, even if the ESI-MS results are encouraging in the effort of filling the gap between solution and solid phase chemistry, a note of caution should be assumed when results are discussed, and further investigation by complementary techniques is recommended.

Notably, modifications in the shape of the L ligand does not significantly influence the resulting structural patterns. However, an electronic effect is observed, determining the presence of a water ligand in the coordination sphere. This behavior appears to be intimately connected with the donor character of each organic ligand. Hence, in the case of the L1 system, it prevents the formation of any other crystalline phase, even from coordinating solvents.

CONCLUSIONS

The supramolecular aggregation in solution of dicyanoaurate with a family of heterometallic Zn^{II} complexes has been demonstrated and characterized with a multitechnique approach. The solution structure of these cationic Zn−Au fragments is coherent with the crystal structures of the compounds obtained from different solvents and a broad platform of ligands, underpinning the general validity of the obtained insights. These tectons seem to show a greater tendency to oligomerize in the case of coordination polymer solid products. Moreover, these phenomena have been observed at low enough concentrations, down to 10^{-4} M, to prevent aggregation due to aurophilic interactions. Taken together, the reported lines of evidence demonstrate that the formation of these bimetallic fragments occurs at the very beginning of the nucleation processes in gold−heterometal systems. Solution-phase preassembly and oligomerization of Au−heterometal units should thus be considered in the crystal engineering of functional Au-based materials, as well as in impure leaching solutions during industrial mining processes.

ASSOCIATED CONTENT

Supporting Information

The Supporting Information is available free of charge at https://pubs.acs.org/doi/10.1021/acs.inorgchem.9b00961.

X-ray structure determination and structural data, X-ray powder patterns, IR and Raman spectra, and thermogravimetric curve (PDF)

Accession Codes

CCDC 1877622−1877630 contain the supplementary crystallographic data for this paper. These data can be obtained free of charge via www.ccdc.cam.ac.uk/data_request/cif, or by emailing data_request@ccdc.cam.ac.uk, or by contacting The Cambridge Crystallographic Data Centre, 12 Union Road, Cambridge CB2 1EZ, UK; fax: +44 1223 336033.

DOI: 10.1021/acs.inorgchem.9b00961
Inorg. Chem. 2020, 59, 203−213

AUTHOR INFORMATION

Corresponding Authors

*E-mail: emanuele.priola@unito.it.
*E-mail: eliano.diana@unito.it.

ORCID

Giorgio Volpi: 0000-0002-9695-9202
Elisa Borfecchia: 0000-0001-8374-8329
Claudio Garino: 0000-0002-7854-6076
Eliano Diana: 0000-0002-7345-8501

Author Contributions

The manuscript was written through contributions of all authors.

Notes

The authors declare no competing financial interest.

ACKNOWLEDGMENTS

The authors gratefully acknowledge Dr. Kirill A. Lomachenko for his competent support during XAS data collection at the BM23 beamline of the ESRF synchrotron, Dr. Anastasia Anceschi for the TGA analysis, and Alessia Giordana for the general experimental support.

REFERENCES

(1) Gil-Rubio, J.; Vicente, J. The Coordination and Supramolecular Chemistry of Gold Metalloligands. *Chem. - Eur. J.* **2018**, *24*, 32−46.
(2) Katz, M. J.; Sakai, K.; Leznoff, D. B. The Use Of Aurophilic And Other Metal-Metal Interactions As Crystal Engineering Design Elements To Increase Structural Dimensionality. *Chem. Soc. Rev.* **2008**, *37*, 1884−1895.
(3) Van Vleet, M. J.; Weng, T. T.; Li, X. Y.; Schmidt, J. R. In Situ, Time-Resolved, and Mechanistic Studies of Metal-Organic Framework Nucleation and Growth. *Chem. Rev.* **2018**, *118*, 3681−3721.
(4) Nangia, A.; Desiraju, G. R. Supramolecular Structures - Reason And Imagination. *Acta Crystallogr., Sect. A: Found. Crystallogr.* **1998**, *54*, 934−944.
(5) Blagden, N.; de Matas, M.; Gavan, P. T.; York, P. Crystal Engineering Of Active Pharmaceutical Ingredients To Improve Solubility And Dissolution Rates. *Adv. Drug Delivery Rev.* **2007**, *59*, 617−630.
(6) El Osta, R.; Frigoli, M.; Marrot, J.; Medina, M. E.; Walton, R. I.; Millange, F. Synthesis, Structure, and Crystallization Study of a Layered Lithium Thiophene-Dicarboxylate. *Cryst. Growth Des.* **2012**, *12*, 1531−1537.
(7) Stavitski, E.; Goesten, M.; Juan-Alcaniz, J.; Martinez-Joaristi, A.; Serra-Crespo, P.; Petukhov, A. V.; Gascon, J.; Kapteijn, F. Kinetic Control of Metal-Organic Framework Crystallization Investigated by Time-Resolved In Situ X-Ray Scattering. *Angew. Chem., Int. Ed.* **2011**, *50*, 9624−9628.
(8) Millange, F.; Medina, M. I.; Guillou, N.; Ferey, G.; Golden, K. M.; Walton, R. I. Time-Resolved In Situ Diffraction Study of the Solvothermal Crystallization of Some Prototypical Metal-Organic Frameworks. *Angew. Chem., Int. Ed.* **2010**, *49*, 763−766.
(9) Hill, J. A.; Thompson, A. L.; Goodwin, A. L. Dicyanometallates as Model Extended Frameworks. *J. Am. Chem. Soc.* **2016**, *138*, 5886−5896.
(10) Alexandrov, E. V.; Virovets, A. V.; Blatov, V. A.; Peresypkina, E. V. Topological Motifs in Cyanometallates: From Building Units to Three-Periodic Frameworks. *Chem. Rev.* **2015**, *115*, 12286−12319.
(11) Fernandez, E. J.; Laguna, A.; Lopez-De-Luzuriaga, J. M. Gold-Heterometal Complexes. Evolution Of A New Class Of Luminescent Materials. *Dalton Trans.* **2007**, 1969−1981.
(12) Cui, G. L.; Cao, X. Y.; Fang, W. H.; Dolg, M.; Thiel, W. Photoinduced Gold(I)-Gold(I) Chemical Bonding in Dicyanoaurate Oligomers. *Angew. Chem., Int. Ed.* **2013**, *52*, 10281−10285.
(13) Lefebvre, J.; Batchelor, R. J.; Leznoff, D. B. Cu[Au-$(CN)_2]_2(DMSO)_2$: Golden Polymorphs That Exhibit Vapochromic Behavior. *J. Am. Chem. Soc.* **2004**, *126*, 16117−16125.
(14) Cairns, A. B.; Catafesta, J.; Levelut, C.; Rouquette, J.; van der Lee, A.; Peters, L.; Thompson, A. L.; Dmitriev, V.; Haines, J.; Goodwin, A. L. Giant Negative Linear Compressibility In Zinc Dicyanoaurate. *Nat. Mater.* **2013**, *12*, 212−216.
(15) Yamasaki, K.; Yasuda, M. Stability of Zinc and Cadmium Complexes with 2,2'-Bipyridine and 1,10-Phenanthroline. *J. Am. Chem. Soc.* **1956**, *78*, 1324−1324.
(16) Ye, B. H.; Tong, M. L.; Chen, X. M. Metal-Organic Molecular Architectures With 2.2 '-Bipyridyl-Like And Carboxylate Ligands. *Coord. Chem. Rev.* **2005**, *249*, 545−565.
(17) Yasuda, M.; Sone, K.; Yamasaki, K. Stability Of Zinc And Cadmium Complexes With Some Methyl Derivatives Of 1,10-Phenanthroline And 2,2′-Bipyridine. *J. Phys. Chem.* **1956**, *60*, 1667−1668.
(18) Irving, H.; Mellor, D. H. 1002. The Stability Of Metal Complexes Of 1,10-Phenanthroline And Its Analogues. Part I. 1,10-Phenanthroline And 2,2′-Bipyridyl. *J. Chem. Soc.* **1962**, *0*, 5222−5237.
(19) Aguiar, P. M.; Katz, M. J.; Leznoff, D. B.; Kroeker, S. Natural Abundance C-13 And N-15 Solid-State NMR Analysis Of Paramagnetic Transition-Metal Cyanide Coordination Polymers. *Phys. Chem. Chem. Phys.* **2009**, *11*, 6925−6934.
(20) Baril-Robert, F.; Li, X. B.; Katz, M. J.; Geisheimer, A. R.; Leznoff, D. B.; Patterson, H. Changes in Electronic Properties of Polymeric One-Dimensional $\{[M(CN)_2]^-\}n$ (M = Au, Ag) Chains Due to Neighboring Closed-Shell Zn(II) or Open-Shell Cu(II) Ions. *Inorg. Chem.* **2011**, *50*, 231−237.
(21) Kappenstein, C.; Ouali, A.; Guerin, M.; Cernak, J.; Chomic, J. Preparation, Structure And Properties Of Dicyano Silver Complexes Of The $M(en)_3Ag_2(CN)_4$ And $M(en)_2Ag_2(CN)_4$ Type. *Inorg. Chim. Acta* **1988**, *147*, 189−197.
(22) Triscikova, L.; Chomic, J.; Abboud, K. S.; Park, J. H.; Meisel, M. W.; Cernak, J. Trinuclear $Cu(pn)_2Ag_2(CN)_4$: Preparation, Crystal Structure Properties (pn = 1,2-Diaminopropane). *Inorg. Chim. Acta* **2004**, *357*, 2763−2768.
(23) Karadag, A.; Aydin, A.; Dede, S.; Tekin, S.; Yanar, Y.; Cadirci, B. H.; Soylu, M. S.; Andac, O. Five Novel Dicyanidoaurate(I)-Based Complexes Exhibiting Significant Biological Activities: Synthesis, Characterization And Three Crystal Structures. *New J. Chem.* **2015**, *39*, 8136−8152.
(24) Xu, G. F.; Liu, Z. Q.; Zhou, H. B.; Guo, Y.; Liao, D. Z. Heteropolymetallic Supramolecular Solid-State Architectures Constructed From Dicyanoaurate Ion, phen, And 3d Metals. *Aust. J. Chem.* **2006**, *59*, 640−646.
(25) Monim-ul-Mehbooba, M.; Ramzan, M.; Ruffe, T.; Lang, H.; Naddem, S.; Ahmad, S. A Zinc(II)-Silver(I) Bimetallic Coordination Polymer Assembled Through Argentophilic and pi-pi Interactions, $\{[Zn(phen)_2(H_2O)\ \{Ag(CN)_2\}[Ag(CN)_2]\cdot MeOH\}_n$ (phen = 1,10-Phenanthroline). *Z. Naturforsch., B: J. Chem. Sci.* **2013**, *68*, 161−167.
(26) Guo, Y.; Ma, Y.; Zhou, N.; Liu, Z. Q.; Wang, Q. L.; Yan, S. P.; Liao, D. Z. Three Dicyanidometallate(I)-based Complexes Incorporating Hydrogen-bonding, pi-pi Packing and d(10)-d(10) Interactions with Auxiliary 2,2 '-Bipyridyl-like Ligands. *Z. Anorg. Allg. Chem.* **2010**, *636*, 865−871.
(27) Qu, J.; Gu, W.; Liu, X. Synthesis, Crystal Structure And Luminescent Properties Of Two Complexes Containing $[Au(CN)_2]^-$ Building Blocks. *J. Coord. Chem.* **2008**, *61*, 618−626.
(28) Ferlay, S.; Bulach, V.; Felix, O.; Hosseini, M. W.; Planeix, J. M.; Kyritsakas, N. Molecular Tectonics And Supramolecular Chirality: Rational Design Of Hybrid 1-D And 2-D H-Bonded Molecular Networks Based On Bis-Amidinium Dication And Metal Cyanide Anions. *CrystEngComm* **2002**, *4*, 447−453.
(29) Dechambenoit, P.; Ferlay, S.; Hosseini, M. W.; Planeix, J. M.; Kyritsakas, N. Molecular Tectonics: Control Of Packing Of Hybrid 1-D And 2-D H-Bonded Molecular Networks Formed Between Bisamidinium Dication And Cyanometallate Anions. *New J. Chem.* **2006**, *30*, 1403−1410.

DOI: 10.1021/acs.inorgchem.9b00961
Inorg. Chem. 2020, 59, 203−213

(30) Codina, A.; Fernandez, E. J.; Jones, P. G.; Laguna, A.; Lopez-De-Luzuriaga, J. M.; Monge, M.; Olmos, M. E.; Perez, J.; Rodriguez, M. A. Do Aurophilic Interactions Compete Against Hydrogen Bonds? Experimental Evidence And Rationalization Based On Ab Initio Calculations. *J. Am. Chem. Soc.* **2002**, *124*, 6781−6786.
(31) Stender, M.; Olmstead, M. M.; Balch, A. L.; Rios, D.; Attar, S. Cation And Hydrogen Bonding Effects On The Self-Association And Luminescence Of The Dicyanoaurate Ion, $[Au(CN)_2]^-$. *Dalton Trans.* **2003**, 4282−4287.
(32) Mendizabal, F.; Pyykkö, P.; Runeberg, N. Aurophilic Attraction: The Additivity And The Combination With Hydrogen Bonds. *Chem. Phys. Lett.* **2003**, *370*, 733−740.
(33) Tiekink, E. R. T. Supramolecular Assembly Of Molecular Gold(I) Compounds: An Evaluation Of The Competition And Complementarity Between Aurophilic (Au···Au) And Conventional Hydrogen Bonding Interactions. *Coord. Chem. Rev.* **2014**, *275*, 130−153.
(34) Piromchom, J.; Wannarit, N.; Pakawatchai, C.; Youngme, S. The heterometallic cadmium-silver complex cis-bis-[dicyanidoargentato(I)-$_k$ N] bis(5,5 '-dimethyl-2,2 '-bipyridyl-$_k$N, N')cadmium(II) monohydrate. *Acta Crystallogr., Sect. C: Cryst. Struct. Commun.* **2013**, *69*, 1136.
(35) Ardizzoia, G. A.; Brenna, S.; Durini, S.; Therrien, B. Synthesis and characterization of luminescent zinc(II) complexes with a N,N-bidentate 1-pyridylimidazo [1,5-a] pyridine ligand. *Polyhedron* **2015**, *90*, 214−220.
(36) Cernak, J.; Gerard, F.; Chomic, J. catena-Poly[silver(I)-μ-(cyano-C:N)-cis-bis-(2,2'-bipyridine-N,N')copper(II)-μ-(cyano-N:C)] Dicyanoargentate(I) Monohydrate. *Acta Crystallogr., Sect. C: Cryst. Struct. Commun.* **1993**, *49*, 1294−1296.
(37) Giordana, A.; Priola, E.; Bonometti, E.; Benzi, P.; Operti, L.; Diana, E. Structural and spectroscopic study of the asymmetric 2-(2'-pyridyl)-1,8-naphthyridine ligand with closed-shell metals. *Polyhedron* **2017**, *138*, 239−248.
(38) Chadwick, B. M.; Frankiss, S. G. Vibrational spectra and structures of some dicyanoaurate(I) complexes. *J. Mol. Struct.* **1976**, *31*, 1−9.
(39) Kettle, S. F. A.; Aschero, G. L.; Diana, E.; Rossetti, R.; Stanghellini, P. L. The Vibrational Spectra of the Cyanide Ligand Revisited: Terminal Cyanides. *Inorg. Chem.* **2006**, *45*, 4928−4937.
(40) Kettle, S. F. A.; Diana, E.; Boccaleri, E.; Stanghellini, P. L. The Vibrational Spectra of the Cyanide Ligand Revisited. Bridging Cyanides. *Inorg. Chem.* **2007**, *46*, 2409−2416.
(41) Perchard, C.; Novak, A. The low-frequency infrared and Raman spectra of ammonia and imidazole complexes of zinc(II) halides. *Spectrochimica Acta Part A: Molecular Spectroscopy* **1970**, *26*, 871−881.
(42) Clark, R. J. H.; Williams, C. S. The Far-Infrared Spectra of Metal-Halide Complexes of Pyridine and Related Ligands. *Inorg. Chem.* **1965**, *4*, 350−357.
(43) Frank, C. W.; Rogers, L. B. Infrared Spectral Study of Metal-Pyridine, -Substituted Pyridine, and -Quinoline Complexes in the 667−150 cm^{-1} Region. *Inorg. Chem.* **1966**, *5*, 615−622.
(44) Postmus, C.; Ferraro, J. R.; Woznizk, W. Low-frequency infrared spectra of nitrogen-ligand complexes of zinc(II) halides. *Inorg. Chem.* **1967**, *6*, 2030−2032.
(45) Di Marco, V. B.; Bombi, G. G. Electrospray mass spectrometry (ESI-MS) in the study of metal−ligand solution equilibria. *Mass Spectrom. Rev.* **2006**, *25*, 347−379.
(46) Weiss, D. T.; Altmann, P. J.; Haslinger, S.; Jandl, C.; Pöthig, A.; Cokoja, M.; Kühn, F. E. Structural diversity of late transition metal complexes with flexible tetra-NHC ligands. *Dalton Trans.* **2015**, *44*, 18329−18339.
(47) Xiao, C.-L.; Wang, C.-Z.; Mei, L.; Zhang, X.-R.; Wall, N.; Zhao, Y.-L.; Chai, Z.-F.; Shi, W.-Q. Europium, uranyl, and thorium-phenanthroline amide complexes in acetonitrile solution: an ESI-MS and DFT combined investigation. *Dalton Trans.* **2015**, *44*, 14376−14387.
(48) Mason, W. R. Electronic structure and spectra of linear dicyano complexes. *J. Am. Chem. Soc.* **1973**, *95*, 3573−3581.
(49) Rawashdeh-Omary, M. A.; Omary, M. A.; Patterson, H. H. Oligomerization Of $Au(CN)_2^-$ And $Ag(CN)_2^-$ Ions In Solution Via Ground-State Aurophilic and Argentophilic Bonding. *J. Am. Chem. Soc.* **2000**, *122*, 10371−10380.
(50) Rawashdeh-Omary, M. A.; Omary, M. A.; Patterson, H. H.; Fackler, J. P. Excited-State Interactions For $[Au(CN)_2^-]_n$ And $[Ag(CN)_2^-]_n$ Oligomers In Solution. Formation Of Luminescent Gold-Gold Bonded Excimers And Exciplexes. *J. Am. Chem. Soc.* **2001**, *123*, 11237−11247.
(51) Avellan, A.; Simonin, M.; McGivney, E.; Bossa, N.; Spielman-Sun, E.; Rocca, J. D.; Bernhardt, E. S.; Geitner, N. K.; Unrine, J. M.; Wiesner, M. R.; Lowry, G. V. Gold nanoparticle biodissolution by a freshwater macrophyte and its associated microbiome. *Nat. Nanotechnol.* **2018**, *13*, 1072.
(52) Uehara, A.; Chang, S. Y.; Booth, S. G.; Schroeder, S. L. M.; Mosselmans, J. F. W.; Dryfe, R. A. W. Redox and Ligand Exchange during the Reaction of Tetrachloroaurate with Hexacyanoferrate(II) at a Liquid-Liquid Interface: Voltammetry and X-ray Absorption Fine-Structure Studies. *Electrochim. Acta* **2016**, *190*, 997−1006.
(53) Tyrsted, C.; Borfecchia, E.; Berlier, G.; Lomachenko, K. A.; Lamberti, C.; Bordiga, S.; Vennestrøm, P. N. R.; Janssens, T. V. W.; Falsig, H.; Beato, P.; Puig-Molina, A. Nitrate−nitrite equilibrium in the reaction of NO with a Cu-CHA catalyst for NH3-SCR. *Catal. Sci. Technol.* **2016**, *6*, 8314−8324.
(54) Chu, I. K.; Shek, I. P. Y.; Michael Siu, K. W.; Wong, W.-T.; Zuo, J.-L.; Lau, T.-C. Synthesis, crystal structure and electrospray ionisation mass spectrometry of a novel one-dimensional cyano-bridged Ni(II)−Au(I) polymer. *New J. Chem.* **2000**, *24*, 765−769.

DOI: 10.1021/acs.inorgchem.9b00961
Inorg. Chem. 2020, 59, 203−213